Cellular proteostasis decline in human senescence

Niv Sabath[1,#], Flonia Levy-Adam[1,#], Anatoly Meller[1], Sharon Soueid-Baumgarten[1] and Reut Shalgi[1,*]

[1] Department of Biochemistry, Rappaport Faculty of Medicine, Technion–Israel Institute of Technology, Haifa 31096, Israel

[#]These authors equally contributed to the work

* Lead author. Correspondence: reutshalgi@technion.ac.il

Abstract

Proteostasis collapse, the diminished ability to maintain protein homeostasis, has been established as a hallmark of nematode aging. However, whether proteostasis collapse occurs in humans has remained unclear. Here we demonstrate that proteostasis decline is intrinsic to human cellular senescence. Using transcriptome-wide characterization of gene expression, splicing and translation, we found a significant deterioration in the transcriptional activation of the heat shock response in stressed senescent cells. Furthermore, phosphorylated HSF1 nuclear localization and organization were impaired in senescence, and alternative splicing regulation was also dampened. Surprisingly, we found a decoupling between different Unfolded Protein Response (UPR) branches in stressed senescent cells. While young cells initiated UPR-related translational and transcriptional regulatory responses, senescent cells showed enhanced translational regulation and ER stress sensing, however they were unable to trigger UPR-related transcriptional responses. Together, our data unraveled a deterioration in mounting stress transcriptional programs upon senescence, and connected proteostasis decline to human aging.

Keywords: Senescence, protein homeostasis, aging, chaperones, UPR, HSF1, Heat shock response

Introduction

Aging is often characterized by the deterioration in the ability to properly respond to external queues. Various systems that are designed to protect the organism against external assaults lose their ability to efficiently mount a full defense when individuals age (Haigis and Yankner, 2010).

Aging is also accompanied by accumulation of damaged proteins. Damaged misfolded proteins are targets of the Protein Quality Control (PQC system), consisting of the proteasome degradation system, and a network of molecular chaperones, whose role is to identify misfolded proteins, refold them, or target them to degradation (Labbadia and Morimoto, 2015a). The chaperone network is also highly induced in response to a variety of proteotoxic stress conditions that lead to increased load of misfolded proteins, and is often able to efficiently maintain protein homeostasis in the face of fluctuating environments (Hartl et al., 2011). However, damaged proteins which are often efficiently dealt with and cleared in young cells, tend to accumulate with age (Vilchez et al., 2014). Accordingly, human diseases of protein misfolding and aggregation, such as Alzheimer's and Parkinson's disease, are often considered age-related, and their prevalence increases dramatically with age (Haigis and Yankner, 2010).

Proteostasis collapse has been found and characterized as a hallmark of aging in nematodes (Ben-Zvi et al., 2009; Taylor and Dillin, 2011). Studies have shown that aging in nematodes is accompanied by a decline in the ability of the organism to deal with misfolded proteins, and mount an efficient proteotoxic stress response (Ben-Zvi et al., 2009). The proteostasis collapse in nematodes occurs at a specific time frame of adulthood and is linked to the reproductive onset (Labbadia and Morimoto, 2015b; Shai et al., 2014; Shemesh et al., 2013). Furthermore, a specific chromatin state has been associated with the phenomenon (Labbadia and Morimoto, 2015b).

But while in nematodes, proteostasis collapse in adulthood is well established, whether a similar phenomenon occurs in mammalian species is still unclear. Studies in mammalian organisms over the years have mainly focused on Hsp70, with mixed conclusions; while several studies have found an impaired stress-mediated Hsp70 induction in aging (Hall et al., 2000; Heydari et al., 1993; Kregel and Moseley, 1996; Liu et al., 1989; Locke and Tanguay, 1996; Westerheide et al., 2009),

as well as impaired DNA binding activity of the HSF1 heat shock transcription factor (Westerheide et al., 2009; Zelin and Freeman, 2015), others have reported that aging has little or no effect on stress-mediated induction of Hsp70 (Carnemolla et al., 2014; Locke, 2000) and a handful of other chaperones.

While many hallmarks of aging support the general notion of proteostasis collapse being a part of human aging, its occurrence in mammalian organisms has not been directly tested on a genome-wide scale. Additionally, there is still debate whether the proteostasis collapse in nematodes is the result of damaged proteins that have accumulated throughout the life of the organism, or whether it is a programmed event (Labbadia and Morimoto, 2015a; Shai et al., 2014; Taylor and Dillin, 2011).

Here we decided to directly test whether proteostasis collapse occurs in human cells. Cellular senescence is a hallmark of aging; the relationship between cellular senescence and human aging is well established(Campisi et al., 2019), and aged mammalian tissues accumulate senescent cells (Campisi and d'Adda di Fagagna, 2007; Lopez-Otin et al., 2013). We therefore chose to use primary human fibroblast cells, which undergo replicative senescence, in order to test the hypothesis of the human proteostasis decline. We grew young cells until they reached replicative senescence, and then exposed the young and senescent isogenic populations to heat shock. We further performed an in-depth characterization of the transcriptome and translatome of these cells in response to heat shock using RNA-seq and ribosome footprint profiling. We found that mammalian senescence shows a significant signature of proteostasis collapse. In an unbiased analysis of our transcriptome data, a group of more than 160 genes, including many chaperones, showed impaired induction upon heat shock in senescent compared to young cells. Furthermore, alternative splicing regulation, which we found to be prevalent upon heat shock in young cells, is highly diminished in senescent cells, further elaborating the scope of the senescent proteostasis decline. We found that the nuclear localization of phosphorylated HSF1, the heat shock transcription factor, is compromised in senescent cells, as well as its nuclear organization. Finally, using ribosome footprint profiling, we revealed that the UPR (Unfolded Protein Response) of the ER was activated in young cells, however the coordination between different UPR branches was impaired in senescent cells; while UPR sensing as well as translational response were enhanced in

senescence, senescent cells were unable to initiate UPR-related transcriptional responses. These results further illuminate the broad molecular scope of the proteostasis decline in mammalian cells, pinpointing to specific transcriptional dynamics impairments.

Results

Heat shock induction of chaperones is compromised in senescent cells

In order to directly test the proteostasis collapse hypothesis in human cells, we utilized young primary human WI38 fibroblasts (passage 24), and grow them until they reached replicative senescence (passage 36 Fig. S1A-C). We then exposed these young and senescent isogenic cells to 2h of acute heat shock at 44ºC. Importantly, fibroblasts undergoing replicative senescence enter a G0 state, and do not proceed through the cell cycle (Campisi and d'Adda di Fagagna, 2007). Since this is one of the major differences between young and senescent cells, we first synchronized the young cells, to enrich for a G1 population and minimize potential cell cycle-related differences, using a starvation-release protocol (see Methods), 24h prior to heat shock. Senescent cells have undergone the same treatment.

Following heat shock (HS), young and senescent cells were harvested and RNA-seq was performed to obtain a transcriptome-wide view of gene expression programs (see Methods, and Table S1 for gene expression data). Differential expression analysis (see Methods) identified about 550 genes which were either differentially expressed upon HS, or between young and senescent cells. We further subjected these differentially expressed genes to unsupervised clustering analysis to determine the major behaviors in the data (Fig. 1A, Table S2A). One of the largest clusters resulting from the analysis consisted of 161 genes that were induced in heat shock in both young and senescent cells, however the extent of induction in senescent cells was compromised (Fig. 1A,B). Importantly, the basal mRNA expression levels of the genes in this cluster was similar between young and senescent cells (Fig. 1C). Interestingly, pathway analysis of the genes in this cluster identified stress response genes and chaperones to be highly enriched (Fig. 2A). We verified the proteostasis collapse behavior of candidate chaperones using realtime qPCR (Fig. S2A,B). Therefore, this cluster presents the molecular manifestation of the proteostasis collapse phenomenon previously defined in nematodes, whereby chaperones are induced during HS in

young cells, but their induction is impaired in senescent cells. We thus termed this cluster – the proteostasis collapse cluster.

We note that the opposite behavior, whereby genes were more induced in senescent cells compared to young cells, was not present in the data; a smaller cluster of 24 HS-upregulated genes were similarly induced in young and senescent cells (Fig. S2D-E, cluster 9).

Since chaperones were enriched among the proteostasis collapse cluster genes, we turned to look at the expression of all chaperones as a group. Chaperones were not basally differentially expressed between unstressed young and senescent cells (Fig. 2B, S3A). Nevertheless, chaperones overall showed a similar pattern of proteostasis collapse, whereby their expression was higher in young cells subjected to HS compared to heat-shocked senescent cells (Fig. S3B,C) and they were more highly induced in young cells in response to HS (Fig. 2C). These trends were evident also when looking at separate chaperone families, with HSP70s, HSP60s and HSP40s all showing a significant proteostasis collapse behavior (Fig. S3D). These results indicate that the proteostasis collapse phenomenon we characterized in human cells is even broader, and spans many of the major chaperone families.

HSF1 nuclear translocation and organization upon heat shock are impaired in senescent cells

The proteostasis decline observed at the level of transcription, which heavily involved chaperones, suggested that the transcriptional heat shock response is compromised in senescent cells. We therefore turned to examine the master regulator of the heat shock response, namely, the HSF1 transcription factor. The overall mRNA levels of HSF1 were no different in young vs. senescent cells (Fig. S4A), and the protein levels were also largely the same (Fig. 3A, S4B,C). HSF1 is known to reside in the cytoplasm under normal conditions, and upon proteotoxic stress it is heavily phosphorylated and translocated to the nucleus, where it induces the transcription of many heat shock genes and chaperones (Akerfelt et al., 2010). We therefore turned to examine phosphorylated HSF1 localization by immunofluorescence in young and senescent cells. Surprisingly, we observed that while phosphorylated HSF1 gave a strong nuclear staining in young cells treated with HS, in senescent cells there was an additional apparent cytoplasmic staining (Fig. 3B,C,S4G). Non-stressed cells, both young and senescent, showed diffused cytoplasmic staining (Fig. S4D). To further quantify the degree of nuclear localization of phospho-HSF1 upon HS, we

performed nuclear-cytoplasmic fractionation in young and senescent HS treated cells, and examined phospho-HSF1 using Western blot (Fig. S4E,F). Non heat-shocked cells showed low cytoplasmic signal for phospho-HSF1, without any nuclear signal. Following heat shock, phospho-HSF1 nuclear levels were high in young cells (Fig. S4E), while in senescent cells the fraction of nuclear phospho-HSF1 was over three-fold lower (Fig. S4E,F). Additionally, we observed that phospho-HSF1 tended to concentrate in a few (1 to 4) distinct nuclear foci in young heat-shocked cells (Fig. 3B,C,S4G), consistent with nuclear stress bodies, as previously characterized in several cell types (Jolly et al., 1999). Senescent cells, however, showed a much more distributed nuclear staining of phospho-HSF1, with significantly higher number of nuclear foci per nucleus, as quantified by image analysis of 3D confocal microscopy images (Fig. S4H,I). Thus, our data suggest that HSF1 nuclear translocation, as well as nuclear organization, upon heat shock are highly compromised in senescent cells.

Proteostasis decline in senescent human cells is evident at the levels of splicing regulation

We have previously shown that heat shock triggers widespread changes at the level of alternative splicing in mouse cells (Shalgi et al., 2014), leading to changes in isoform expression, including extensive yet selective intron retention (Shalgi et al., 2014). We therefore decided to explore alternative splicing regulation in the human senescence system. We performed alternative splicing analysis using MISO (Katz et al., 2010), an algorithm that quantifies the change in the inclusion fraction of a splicing event (Percent Spliced In, PSI), and provides a Bayes Factor (BF) as an estimate for the significance of the change. We analyzed a variety of previously annotated isoform type changes (Katz et al., 2010), including exon skipping, intron retention, alternative 5' and 3' splice site usage, and alternative last exon usage, and quantified the significance of their changes either upon HS in young or senescent cells, or between young and senescent cells. We further defined strict cutoffs in order to enforce replicate reproducibility of the significance of change in alternative splicing (see Methods). Overall, we found 268 significantly changing annotated alternative splicing events in our system (Fig. 4A, S5A-D). There were very few significant changes in alternative isoforms between unstressed young and senescent cells, and the majority of significant alternative splicing changes occurred upon HS (Fig. S5E). Surprisingly, we found that, in all alternative splicing categories examined, senescent cells show very few significant splicing

changes upon HS, 44-81% less than in young cells (Fig. 4A). We further used clustering analysis to look at the patterns of alternative splicing changes, and observed, again, a clear behavior of proteostasis decline, whereby PSI values show a robust change upon HS in young cells, and changes were much weaker in senescent cells (Fig. S5D). We further examined global intron retention, as in (Shalgi et al., 2014), and found that, here too, senescent cells have 70% less retained introns upon HS than young cells (Fig. 4B, S5F). All of these trends were robust to the choice of parameters (see Methods and Fig. S5E). Thus, our data suggested that alternative splicing regulation upon HS is largely impaired in senescent cells, further expanding the scope of the molecular proteostasis decline.

Exploring translational control in the young and senescent heat shock response

We next turned to map the cellular translatome in young and senescent cells in response to heat shock, in order to explore potential regulation at the level of translation. To that end, we performed ribosome footprint profiling (or Ribo-seq) on the same young and senescent cells described above, before or after exposing them to 2h of HS (see Methods). Translation level changes largely mirrored mRNA expression changes for the major differentially expressed RNA-seq clusters that we have identified above (Fig. 1A, S2D and S6A). Differential expression analysis of the translation data resulted in more differentially expressed genes than transcript level data; we found 1222 mRNAs (Fig. 5) with differential translation compared to 548 differentially expressed mRNAs identified by RNA-seq (Fig. 1A). Overall, the two sets of differentially translated or expressed genes partially overlapped (Fig. S6B). Clustering analysis (Table S2) revealed that the proteostasis collapse cluster was also evident at the level of translation (Fig. 5, red cluster), and that the translation proteostasis collapse cluster highly overlapped with the RNA-seq proteostasis collapse cluster (Fig. S6B). Here too, there was no difference in the basal translation levels of the mRNAs in the proteostasis collapse cluster between young and senescent cells (Fig. S6C,D). The translation proteostasis collapse cluster was enriched with stress response genes and chaperones (Table S3B), similarly to the RNA proteostasis collapse cluster.

Within the translationally differentially expressed gene group, our clustering analysis has identified a second cluster of HS induced genes (Fig. 5,S6B, orange cluster), with about 150

mRNAs which were HS-induced in senescent cells slightly more than in young cells (Fig. S6F). These mRNAs were enriched with RNA binding proteins, and with extracellular matrix and extracellular exosome genes (Table S3B). Here too, mRNAs did not show any basal difference in their translation between young and senescent cells (Fig. S6C,D).

Loss of coordination between UPR regulatory branches in senescent cells

Our clustering analysis of differentially translated mRNAs has identified two large clusters of HS repressed mRNAs (Fig. 5, blue and black clusters). Both of these clusters were largely driven by translational repression (Fig. S6B,E,F, clusters number 15 and 2 respectively). But while the blue cluster showed similar degrees of repression upon HS in young and senescent cells (Fig. S6F), the black cluster mRNAs were much more repressed in senescent cells (Fig. 6A). It is therefore denoted as the senescence-enhanced HS repression cluster. Pathway analysis revealed that this cluster is highly enriched with glycoproteins, disulfide bond containing proteins, and membrane proteins (Fig. 6B, Table S4); which represent the major classes of ER targets. Widespread repression of ER targets has been previously reported by us and others (Gonen, 2019; Guan et al., 2017; Reid et al., 2014) to be a hallmark of the UPR, representing a significant translational regulatory response mediated by PERK (Gonen, 2019). We therefore reasoned that the HS treatment in our experiment has induced the UPR. Indeed, examination of the set of mRNAs that were previously identified as the PERK-dependent translational repression UPR signature (Gonen, 2019), which was found to be highly enriched for ER targets, confirmed that this set of mRNAs was significantly repressed in both young and senescent cells in response to HS, however repression was substantially greater in senescent cells (Fig. S7A,B). Importantly, here too, repression occurred at the level of translation (Fig. S7A,B). Previously, we have shown that the PERK-mediated repression of ER targets as part of the UPR involved eIF2α phosphorylation (Gonen, 2019). We confirmed that eIF2α phosphorylation occurred in both young and senescent cells upon HS, to a similar extent (Fig. S7C,D). ATF4 ORF translation, another UPR hallmark event downstream of PERK and phospho-eIF2α (Pavitt and Ron, 2012), was induced to a similar extent in young and senescent heat-shocked cells (Fig. S7E-F). Therefore, it seems that the PERK branch of the UPR is activated in both young and senescent stressed cells. We thus sought to examine other UPR branches in this system.

To further explore the induction of the IRE1 branch of the UPR, we examined the splicing profile of XBP1, whose cytoplasmic splicing by IRE1 is considered to be one of the primary steps in ER stress sensing (Pavitt and Ron, 2012). To that end, we quantified the degree of splicing in each sample using the MISO algorithm (Katz et al., 2010). First, there was very little XBP1 splicing in both young and senescent unstressed cells, verifying that senescent cells are not under basal ER stress. Upon stress in young cells, XBP1 is partially spliced, to a level of about 64% (Fig. 6C, S7G). In senescent cells, however, XBP1 splicing was enhanced, to a level of about 88%.

Therefore, it seems that senescent cells sense protein misfolding in the ER that occurs in heat shock to an even higher degree than young cells. They also activate the PERK branch and its translational outputs, both translational enhancement (ATF4, Fig. S7E,F) and repression (ER targets, Fig. 6A,B, Fig. S7A,B), to a similar, or even higher extent than in young cells. Nevertheless, in order to transition into the adaptive phase of the UPR, transcriptional activation of the target genes of the two transcriptional UPR branches, namely the ATF6 and XBP1-s (XBP1-spliced) transcription factors (Zhang and Kaufman, 2004), should take place. We therefore examined the transcriptional outputs of these two branches, by looking at a set of bona-fide ATF6 and XBP1-s target genes previously defined by Shoulders et al. (Shoulders et al., 2013). Strikingly, we found that while ATF6 target genes were significantly induced in young cells both transcriptionally and translationally (Fig. 6D, $p=1.7^{-5}$ and $p=1.1^{-3}$ at the mRNA expression and translation levels respectively), they were not induced at all in senescent cells (Fig. 6E, p=0.87 and p=0.77 at the expression and translation levels respectively). A similar trend emerged when we examined the set of bona-fide XBP1-s targets (Shoulders et al., 2013) (Fig. S7H,I).

Hence, our data suggest that while young cells are able to sense ER protein misfolding upon HS, and initiate both transcriptional activation as well as translational activation and repression programs as part of the UPR, senescent cells show decoupling of the different UPR arms; Their IRE1-mediated stress sensing (as quantified by XBP1 splicing), and PERK-mediated translational regulation are both intact, or even enhanced, however they fail to activate the UPR transcriptional branches of ATF6 and XBP1-s. Thus, our combined analysis of transcription and translation data unraveled yet another level of proteostasis decline in senescent cells. Furthermore, our data

revealed what seems to be a more general deterioration in the ability of senescent cells to initiate the required transcriptional reprogramming upon protein misfolding stress, by HSF1, ATF6 and XBP1-s, an essential step in the cellular ability to cope with and adapt to stress.

Discussion

An impaired cellular stress response during aging has long been thought to contribute to age-related diseases (Labbadia and Morimoto, 2015a; Lopez-Otin et al., 2013). In nematodes, the phenomenon of proteostasis collapse upon aging is well established (Ben-Zvi et al., 2009), and has been shown to initiate at the onset of reproduction (Labbadia and Morimoto, 2015b; Shemesh et al., 2013). Furthermore, multiple evidences suggest that it is a programmed event, related to overall organismal reproductive capacity and fitness (Labbadia and Morimoto, 2015a; Shemesh et al., 2013). Here, we report the first genome-wide quantification of transcriptional and translational responses to heat shock in senescent human cells. Our results show that proteostasis decline occurs in human primary fibroblasts upon replicative senescence. It is a widespread phenomenon including a reduced transcriptional induction of many chaperones and impairment of splicing regulation. Proteostasis collapse in nematodes has been shown to represent an organismal level phenomenon. Furthermore, the nature, extent, and onset of the nematode proteostasis collapse can be modulated by external signals, in a non-autonomous fashion (Labbadia and Morimoto, 2015a; Taylor and Dillin, 2011). Our data showed that the proteostasis decline in human senescence occurs in a cell-autonomous manner, namely, it is an intrinsic characteristic of cells. These findings further support the notion that this is a programmed phenomenon, rather than a mere consequence of accumulation of damaged proteins throughout life. The question of the consequences of the human cellular senescence proteostasis decline at the organismal level is very intriguing, although highly complex. The connection between human aging and senescence has been well established for many years (Campisi et al., 2019). Our data therefore imply that indeed, accumulating population of senescent cells in the aged human organism experience proteostasis decline. To examine the potential link between our findings and human aging, we analyzed a dataset of chaperone signatures previously identified as consistently altered in aged human brains (Brehme et al., 2014). Interestingly, we found that while the levels of both aging brain-induced and -repressed chaperones were similar between young and senescent cells (Fig. 7, S8), chaperones

identified as repressed in aging brains, but not those that were induced, showed the proteostasis decline behavior in senescent human cells; namely, they were significantly more induced upon heat shock in young cells than in senescent cells ($p=8.5^{-7} – 7.3^{-4}$, Fig. 7A-C, S8A-C). Potentially, diminished steady state expression of a subset of chaperones in aged brains is further accompanied by the inability to induce these chaperones upon proteostasis assaults. This could be the manifestation of a combined overall effect of programmed proteostasis decline, as well as proteostasis deterioration due to gradual accumulation of damaged proteins that burden the chaperone network upon human aging. Therefore, our study represents a first step towards generalizing the understanding of proteostasis collapse in human aging, and future work will further delineate the cell-autonomous vs. non-autonomous nature of the phenomenon in aged mammalian organisms.

Our evidence point to stress sensing being intact in senescent cells, as shown by greater activation of the IRE1-mediated XBP1-splicing branch of the UPR (Fig. 6C,S7G). Additionally, we observed an intact translational regulatory response, evident by enhanced activation of the PERK-mediated UPR translation signature (Fig. 6A,B,S7A,B), as well as eIF2α phosphorylation (Fig. S7C,D), and ATF4 ORF translation (Fig. SE,F). As primary fibroblasts secrete many extracellular matrix proteins, they are apparently more sensitive to other forms of proteotoxicity, including HS, and therefore activated the UPR. Importantly, unstressed senescent cells did not show basal UPR activation, as evident by similar expression levels of BiP (Hspa5, Table S1), and low levels of XBP1 splicing (Fig. 6C). Furthermore, senescent cells in general, and senescent fibroblasts in particular, are highly secretory (Campisi, 2013), which could explain why their sensing and translational responses are both aggravated in response to HS. However, eliciting transcriptional responses was compromised in senescent cells not only for HSF1, but also for the UPR transcriptional branches mediated by ATF6 and XBP1-s. Interestingly, nematode UPR activation is also deteriorated during aging (Ben-Zvi et al., 2009; Taylor and Dillin, 2013), however in contrast to human senescence, nematodes fail to activate the IRE-1 branch altogether (Taylor and Dillin, 2013). Our evidence suggest that senescent human cells can initiate the UPR, however their ability to transition to the adaptive stage of the UPR, where transcriptional programs need to take place, is diminished. Taken together, these evidences suggest that perhaps certain properties required for dynamic stress transcriptional responses are overall declined in senescence.

What could be the underlying mechanism for a general deterioration in the ability to elicit stress transcriptional responses in senescent cells? Our data point to two potential, not mutually exclusive, possibilities discussed below.

Previous studies have shown diminished DNA binding activity of HSF1 in human senescence (Westerheide et al., 2009). Additionally, HDAC1 has been shown to attenuate HSF1 DNA binding activity upon heat shock in senescent MEFs (Zelin and Freeman, 2015). Our data adds two additional dimensions to explain HSF1 deteriorated transcriptional activity: reduced nuclear localization, and disordered nuclear organization.

An interesting possibility is that chromatin structure in human senescence in particular, and during aging in general, is altered in a manner that disables efficient dynamic changes in opening of chromatin regions, either globally, or specifically at regions essential for stress responses, thereby affecting access of HSF1 and other stress transcription factors to their DNA targets upon stress. In nematodes, proteostasis collapse was accompanied by increased H3K27me3 chromatin marks at several chaperone gene loci (Labbadia and Morimoto, 2015b). Additionally, the expression of the histone demethylase *jmjd-3.1* is decreased in aged nematodes, while its overexpression maintained proper induction of the heat shock response upon aging (Labbadia and Morimoto, 2015b), and led to increased lifespan (Merkwirth et al., 2016). Similar trends of reduction in activating histone marks and induction of repressive marks have been shown in flies (Wood et al., 2010) and fish (Baumgart et al., 2014), supporting the notion that a closed chromatin state at chaperone gene loci, or perhaps more globally, may confound the deteriorated induction of the heat shock response upon aging.

In mammals, however, characterization of senescence and aged chromatin states has yielded a highly complex picture. The chromatin landscape of senescent cells seems to be very different than the pre-senescent state (Sen et al., 2016). While Senescence-Associated Heterochromatin Foci (SAHF), regions of highly dense heterochromatin, were shown to be a hallmark of human senescence (Narita et al., 2003; Sen et al., 2016), other studies reported a general decrease in histone content in senescent and aged cells (Ivanov et al., 2013; O'Sullivan et al., 2010), and some histone variants were shown to be upregulated (Rai et al., 2014). Reorganization in the landscape of several activating and repressing histone marks has also been observed (Sen et al., 2016). Finally, transcription of satellite repeats has been shown to occur after cells enter senescence (De Cecco et al., 2013). Interestingly, HSF1 localization to nuclear foci

upon heat shock, observed in young cells (Fig. 3B,C,S3G), has been previously demonstrated to occur at satellite III regions (Jolly et al., 2002). Our observation of disorganized HSF1 nuclear foci might be explained by an altered chromatin state which allows more pervasive satellite repeat expression prior to stress, thus leading to redistribution of HSF1 into numerous foci in senescent cell.

Nuclear Lamin disfunction has also been linked to aging and senescence; Lamin B shows decreased expression upon senescence (Freund et al., 2012; Shimi et al., 2011), with major consequences on nuclear and genome organization (Shah et al., 2013), and Lamin A/C mutations causing premature aging in HGPS alter nuclear structure, transcriptional deregulation, and chromatin organization (Burtner and Kennedy, 2010; Prokocimer et al., 2013). More recently, senescent cells were shown to contain cytoplasmic blebs of chromatin (Dou et al., 2015; Ivanov et al., 2013). Our results on HSF1 diminished nuclear localization and increased cytoplasmic localization fit well with the notion of compromised nuclear integrity in senescence. If nuclear integrity is compromised, together with reorganized chromatin that disfavors optimal stress transcription factor binding, HSF1, and potentially other transcription factors, will remain unbound to chromatin and therefore might more easily exit back into the cytoplasm.

Future studies will unravel the full extent of nuclear integrity deterioration upon senescence, and the link between the altered chromatin landscape to the deterioration in dynamic stress response activation in human senescence and aging.

Materials and Methods

Cell culture and stress

WI38 human lung fibroblasts were grown in MEM Earl's medium, 10% serum, L-glutamine, 1% Na-pyruvate, 1% nonessential amino acids and 1% penicillin/streptomycin solution. For the synchronization of the cell cycle, cells were plated on 15 cm plates at a confluency of $1.5x10^6$ for senescent or $1.3x10^6$ for young cells. The next day, the cells underwent starvation (starvation medium was MEM Earl's medium +1% penicillin/streptomycin solution) for 24 h followed by recovery in regular growth media for another 24 h. After recovery cells were subjected to stress, (heat shock at 44^0C, for 2 h) and then harvested in Lysis Buffer (20mM Hepes pH 7, 100mM KCl,

5mM MgCl2, 0.5% Na DOC, 0.5% NP-40, 1mM DTT, Protease inhibitors (Roche)). Samples were used for RNA-Seq or Ribo-Seq.

RNA-Seq library preparation

RNA was isolated from collected samples using the TRIZOL reagent (Thermo) following treatment with Turbo DNase and phenol chloroform precipitation. After quality control check, the samples were subjected to Illumina kit (TruSeq RNA) for library preparation.

Ribosome footprint profiling library preparation

Ribosome footprint profiling was performed as described in (Shalgi et al., 2013) with the following modifications: Following heat shock, cells were lysed directly on the plate on ice for 10 minutes using the Lysis Buffer (see above) without Cycloheximide. Then the samples were treated with 20µl Turbo DNase for 5 minutes at 25^0C while rotating. At this point 10% of the lysate was taken for RNA-seq (see above). Nuclei were removed with 10min centrifugation at maximum speed at 4^0C and supernatant was retained. Then, 8 µl NEB RNase If (NEB M0243S) per OD260 of ~10 was added in 2ml of lysis buffer, and was rotated for 55min at room temperature. Ribosomes were pelleted using a sucrose cushion (10ml lysis buffer layered on top of 12.5 ml cushion: 20 mM HEPES pH 7, 100 mM KCl, 5 mM MgCl2, 0.5 M Sucrose), by ultracentrifugation at 60K RPM for 1 hour and 50 minutes, at 4^0C with a Ti70 rotor.

RNA-Seq analysis

RNA-Seq reads were filtered for rRNAs, tRNAs, microRNAs, and snoRNAs using STAR (Dobin et al., 2013). The remaining reads were mapped to hg19 version of the human genome using STAR (Dobin et al., 2013). Expression levels were quantified using RSEM (Li and Dewey, 2011) to produce gene level quantification TPM (Transcript Per Million) values. TPM values were then averaged between sample replicates.

Ribosome profiling analysis

Ribosome footprint reads were trimmed to a maximal length of 34 and polyA sequences which were generated in the polyA tailing step of the ribosome footprint profiling protocol were removed, such that footprints of lengths 22-34 were considered. Reads were filtered for rRNAs, tRNAs,

microRNAs, and snoRNAs using STAR (Dobin et al., 2013). The remaining reads were mapped to hg19 version of the genome using RefSeq modified CDSs; Transcripts shorter than 100 nucleotides were filtered out and 30 nucleotides were clipped from the start and end of each CDS before mapping, similarly to Ingolia (Ingolia et al., 2012). Expression levels (mRNA TPM) were quantified using RSEM (Li and Dewey, 2011) after mapping to clipped CDSs using Bowtie2 (Langmead and Salzberg, 2012). TPM values were averaged between sample replicates.

Differential expression analysis

We applied the R package DESeq2 (Love et al., 2014) on the read-count tables resulting from RSEM to identify mRNAs that were differentially expressed (DEGs) between pairs of samples (we used FDR-corrected p-value < 0.05). We compared either between young and senescent, or between either young or senescent cells before and after heat shock treatments, and all DEGs found in at least one comparison were considered for further analysis.

Hierarchical clustering

Lowly expressed mRNAs with TPM value below four across all samples were filtered out. TPM values of all remaining genes were thresholded to four. Hierarchical clustering (using MATLAB) of gene expression levels was done based on spearman correlation between log2 TPM values of mRNAs across samples. Clustergrams were displayed after gene-wise Z-score normalization for visualization purposes.

Functional Enrichment analysis and gene groups

Pathway enrichment analyses were conducted using RDAVIDWebService R package (Fresno and Fernandez, 2013), using all expressed genes as background. Pathways with Benjamini corrected p-value <0.05 were designated as significantly enriched.

Chaperone list (Fig. 2B,C, S3A,B) was manually curated (Table S5), or taken from Brehme et al. supplementary information (Brehme et al., 2014) (Fig. S3C), for all cytosolic chaperones (excluding the ER and MITO families), and excluding the TPR, PFD families. Additionally, chaperone families HSP70, HSP40 and HSP60 (Fig. S3D) were taken from Brehme et al. (Brehme et al., 2014) supplementary information. XBP1 and ATF6 targets were defined by Shoulders et al. (Shoulders et al., 2013) following specific direct activation of XBP1 or ATF6 (termed XBP1 and

ATF6 targets). PERK-dependent UPR repression signature gene set was defined according to Gonen et al. (Gonen, 2019). Groups of chaperones significantly altered (induced or repressed) in aged brains (in Postcentral Gyrus, Prefrontal Cortex and Superior Frontal Gyrus, Fig. 7, S8) were taken from Brehme et al. (Brehme et al., 2014) supplementary information.

For all gene group comparisons using CDF plots, two-sample Kolmogorov-Smirnov goodness-of-fit test (KS test) was performed for every group compared to the corresponding background distribution, using all expressed genes as background, and p-values <0.01 were designated as significant. In some cases, the same test was applied between two groups of interest (indicated). Significant p-values are indicated on the top of the CDF plots, or in the figure legends.

Nuclear-cytoplasmic fractionation and WB analysis

In order to separate between nuclear and cytoplasmic fractions we used NE-PER Nuclear and Cytoplasmic Extraction Reagents (Thermo Scientific). Cells were plated on 6-well plates and after 2h HS were collected in PBS, centrifuged and cell pellets were frozen. The fractionation procedure was performed following manufacturer's instructions. At the end, samples were subjected to WB with anti phospho-HSF1 (S326) antibody (Abcam, AB-ab76076) and anti Actin-b (MBL, 8691001), or anti-HSP90 (Abcam, ab13492). Additional antibodies used for WB: anti phospho-eIF2α (Cell Signaling, CST-9721S) and anti eIF2α (Cell Signaling, CST-5324S) in Fig. S7C, and anti-HSF1 (10H8 clone, Stressmarq, SMC-118D) in Fig. 3A. WB bands densitometry were quantified using Fiji.

HSF1 immunofluorescence

For Immunofluorescence (IF), young or senescent cells were plated on coverslips in 12-well plates. On the day of the experiment, the cells were subjected to a 2h HS and then were fixed in 4% PFA. The antibodies used were: anti phospho-HSF1 (S326) antibody (Abcam, AB-ab76076) at 1:200 dilution, secondary anti-rabbit antibody (Jackson Laboratories) at 1:400 dilution. For the detection of nuclei the coverslips were incubated with 1 ug/ml DAPI in PBS for 5 min before mounting. Images were taken with Zeiss LSM700 laser scanning confocal microscope. Image analysis for quantification of the number of phospho-HSF1 nuclear foci was performed using Imaris software scripts on 3D confocal microscopy images (x40 magnification), with 6-8 fields for each of either

young HS or senescent HS cells. Two independent replicate experiments gave similar results (Fig. S4H,I).

Alternative splicing analysis

We used MISO (Katz et al., 2010) to examine differential alternative splicing upon HS in young and senescent cells, or between young and senescent cells. MISO GFF3 annotation files for hg19 for skipped exons, alternative 3' and 5' splice sites, alternative last exons, and retained introns were downloaded from the MISO website (https://miso.readthedocs.io/en/fastmiso/). GFF3 annotation file of all introns was produced using in-house scripts. All GFF3 annotations were indexed using the index_gff procedure from the MISO package. For each sample (each with two replicates), MISO was run using default settings. To assess significant differences between samples, we ran the procedure compare_miso between samples and between replicates. We denoted an event as significant if the Bayes Factors (BFs) for the comparisons between replicates were below 4 and BFs for the comparisons between different samples were greater than 8. E.g., BF of Young1 – Young2<4 and Young-HS1 – Young-HS2 < 4 and Young1 – Young-HS1>8 and Young2 – Young-HS2 >8. All reported trends were robust to different BF cutoffs, as observed in Fig. S5E.

Acknowledgements

We thank Edith Suss-Toby and Shani Bendori from the Bioimaging center of the Faculty of Medicine Biomedical Core Facility at the Technion, for their assistance with image analysis and the Imaris software. We thank Herman Wolosker for critical reading of the manuscript. This project has received funding from the European Research Council under the European Union's Horizon 2020 programme Grant 677776.

Authors Contributions

R.S. conceived and supervised the study. F.L.A. performed all experiments. S.S.B helped with Fig. S4E,F and S7C. N.S. performed all computational data analysis, with help from A.M., who also performed the analyses for Fig. 7 and S8. R.S wrote the paper with help from N.S. and input from all other authors.

Competing Interests

The authors declare no competing interests.

Data Availability

All RNA-seq and ribosome footprint profiling data were deposited in GEO, GSE124609.

Supplementary Information

Supplementary Information file containing Figures S1-S8.

Supplementary Tables : Tables S1-S5.

Figure Legends

Figure 1: mRNA expression analysis of heat shock treated young and senescent cells.

(A) Hierarchical clustering analysis of 548 mRNAs with significant expression difference (using DESeq2 FDR-corrected p-value < 0.05) in at least one comparison between different sample types. The figure shows a gene-wise normalized Z-score heatmap of the log2 expression (RNA-seq TPM) values. The proteostasis collapse cluster, a cluster with induced expression levels upon HS, which is attenuated in senescent cells, is marked by a red box. Of the 161 mRNAs in this cluster, there are 27 chaperones, out of 28 differentially expressed chaperones identified. (B) CDF plot of the log2 expression fold change (HS/Control RNA-seq TPM) for mRNAs in the proteostasis collapse cluster, shown for senescent (blue) and young (red) cells. Gray lines depict the background distributions (bg), corresponding to all expressed genes in senescent (solid line) and young cells (dashed line). The log2 fold change is greater in young than in senescent ($p=4.3^{-10}$, KS test). (C) No significant difference between basal expression (log2 RNA-Seq TPM) of the mRNAs in the proteostasis collapse cluster in young vs. senescent cells (p=0.7, KS test).

Figure 2: Heat shock-mediated induction of chaperones is impaired in senescent cells.

(A) Functional enrichment analysis of the proteostasis collapse cluster performed using DAVID, showed that the cluster is characterized by stress response genes and chaperones. (B) No significant difference between mRNA expression levels (log2 RNA-Seq TPM) of all chaperones in young vs. senescent samples (p=1, KS test). Manually curated chaperones list (157 chaperones)

is in Table S5, similar results obtained with the chaperone list from Brehme et al. (Brehme et al., 2014), see Fig. S3C. (C) CDF plot of the difference between the HS fold changes (log2 TPM HS/Control, denoted as LFC) between young and senescent cells, demonstrating that chaperones are overall more highly induced in young cells ($p = 1.4^{-9}$, KS test).

Figure 3: Heat shock-mediated nuclear localization and organization of HSF1 are hampered in senescent cells.

(A) The total levels of HSF1 in young and senescent cells are very similar (see also Fig. S4A-C). (B) Immunofluorescence (IF) staining of phospho-HSF1 in young and senescent heat shocked cells show increased cytoplasmic staining in senescent cells. Additionally, while most young cells show 1-4 single bright nuclear foci of phospho-HSF1 upon HS, most senescent cells show many disorganized foci of phospho-HSF1. (C) Confocal 3D imaging of phospho-HSF1 in young and senescent heat-shocked cells revealed a closer look of the nuclear foci organization in young cells, and its impairment in senescent cells. Additional images and quantification of the number of foci is shown in Fig. S4G-I.

Figure 4: Regulation of alternative splicing following heat shock is highly diminished in senescent cells.

Number of differential alternative splicing (A) and intron retention (B) isoforms upon HS in young (red) and senescent (blue) cells. Alternative splicing and annotated retained introns events were initially downloaded from the MISO annotation collection (Katz et al., 2010). An event was denoted significant if the Bayes Factor (BF) of each HS vs. Control comparisons (in the two replicates) were above eight and the BF of replicate comparisons (Control1 vs. Control2 and HS1 vs. HS2) were below four. The trend is robust to varying BF cutoffs, as shown in Fig. S5E.

Figure 5: Exploring translational control in the young and senescent heat shock response using ribosome footprint profiling.

Hierarchical clustering analysis of 1222 mRNAs with significant expression difference (DESeq2 FDR-corrected p-value < 0.05) in at least one comparison between samples. The figure shows a gene-wise Z-score normalized heatmap of the translation (log2 Ribo-Seq TPM) values. The red box marks a cluster with increased expression level upon HS, which is attenuated in senescent

cells, in line with the proteostasis collapse mRNA-level cluster above (Fig. 1). Of the 189 genes in this cluster, there are 30 chaperones out of 39 DEG chaperones. The blue and black boxes mark two HS repression clusters, which are both translation specific.

Figure 6: Loss of coordination between UPR branches in senescent cells upon heat shock.

(A) CDF plot of the log2 translation fold-changes (HS/Control, Ribo-seq TPM) for mRNAs from the senescence enhanced HS repression cluster (Fig. 5, black cluster), shown for senescent (blue) and young (red) cells. Gray lines depict the corresponding CDF plots for the background distribution, i.e. all translated mRNAs in senescent (solid grey line), or young (grey dashed line) cells. The repression is significantly stronger in senescent than young cells ($p=5.9^{-44}$, KS test). (B) Functional enrichment analysis of the senescence enhanced HS repression cluster was performed using DAVID, and showed that the cluster is highly enriched with ER targets. Full list of annotations is available in Table S4. (C) Splicing plot (Sashimi plot (Katz et al., 2010)) of XBP1 exon four (of the unspliced isoform). The percent spliced isoform, PSI values, of the spliced XBP1 isoform for all samples was quantified using MISO (Katz et al., 2010) are indicated: 2%, 4% (senescent) 85%, 91% (senescent HS) 2%, 14% (young) 66%, 62% (young HS). Significance of change was quantified by MISO and resulted in the following Bayes factors (BFs): BFs for HS vs. Control samples: 1012, for all comparisons. BFs for senescent vs. young: 1.9,0.1, indicating no basal difference in the amount of XBP1-spliced. BFs for senescent-HS vs. young-HS: 14717,3.810. (D, E) CDF plots of the log2 fold change (HS/Control) of the set of bona-fide ATF6 target genes (taken from (Shoulders et al., 2013)) demonstrate their significant induction upon HS in young cells (D) both at the mRNA (red) and the translation (blue) levels ($p=1.7^{-5}$, and $p=1.1^{-3}$ for mRNA expression and translation respectively, using KS test). No induction was observed in senescent cells (E, p=0.87 and p=0.77 for mRNA expression and translation respectively, using KS test).

Figure 7: Repressed chaperone signature from aged human brains show proteostasis collapse behavior in human senescence.

(A-C) Age-repressed chaperones were taken from Brehme et al. (Brehme et al., 2014), as defined for three different brain regions. CDF plots depict the log2 expression fold changes of this signature in Young/Senescent, either in untreated (blue) or heat-shocked (red) cells. These

chaperones show a proteostasis collapse behavior in human senescent cells: they were significantly more induced in heat shock in young vs. senescent cells, and therefore the HS curve is significantly shifted. On the other hand, aged-induced chaperones from the same tissues show no significant difference (see Fig. S8).

References

Akerfelt, M., Morimoto, R.I., and Sistonen, L. (2010). Heat shock factors: integrators of cell stress, development and lifespan. Nat Rev Mol Cell Biol *11*, 545-555.

Baumgart, M., Groth, M., Priebe, S., Savino, A., Testa, G., Dix, A., Ripa, R., Spallotta, F., Gaetano, C., Ori, M.*, et al.* (2014). RNA-seq of the aging brain in the short-lived fish N. furzeri - conserved pathways and novel genes associated with neurogenesis. Aging Cell *13*, 965-974.

Ben-Zvi, A., Miller, E.A., and Morimoto, R.I. (2009). Collapse of proteostasis represents an early molecular event in Caenorhabditis elegans aging. Proc Natl Acad Sci U S A *106*, 14914-14919.

Brehme, M., Voisine, C., Rolland, T., Wachi, S., Soper, J.H., Zhu, Y., Orton, K., Villella, A., Garza, D., Vidal, M.*, et al.* (2014). A chaperome subnetwork safeguards proteostasis in aging and neurodegenerative disease. Cell Rep *9*, 1135-1150.

Burtner, C.R., and Kennedy, B.K. (2010). Progeria syndromes and ageing: what is the connection? Nat Rev Mol Cell Biol *11*, 567-578.

Campisi, J. (2013). Aging, cellular senescence, and cancer. Annu Rev Physiol *75*, 685-705.

Campisi, J., and d'Adda di Fagagna, F. (2007). Cellular senescence: when bad things happen to good cells. Nat Rev Mol Cell Biol *8*, 729-740.

Campisi, J., Kapahi, P., Lithgow, G.J., Melov, S., Newman, J.C., and Verdin, E. (2019). From discoveries in ageing research to therapeutics for healthy ageing. Nature *571*, 183-192.

Carnemolla, A., Labbadia, J.P., Lazell, H., Neueder, A., Moussaoui, S., and Bates, G.P. (2014). Contesting the dogma of an age-related heat shock response impairment: implications for cardiac-specific age-related disorders. Hum Mol Genet *23*, 3641-3656.

De Cecco, M., Criscione, S.W., Peterson, A.L., Neretti, N., Sedivy, J.M., and Kreiling, J.A. (2013). Transposable elements become active and mobile in the genomes of aging mammalian somatic tissues. Aging (Albany NY) *5*, 867-883.

Dobin, A., Davis, C.A., Schlesinger, F., Drenkow, J., Zaleski, C., Jha, S., Batut, P., Chaisson, M., and Gingeras, T.R. (2013). STAR: ultrafast universal RNA-seq aligner. Bioinformatics *29*, 15-21.

Dou, Z., Xu, C., Donahue, G., Shimi, T., Pan, J.A., Zhu, J., Ivanov, A., Capell, B.C., Drake, A.M., Shah, P.P.*, et al.* (2015). Autophagy mediates degradation of nuclear lamina. Nature *527*, 105-109.

Fresno, C., and Fernandez, E.A. (2013). RDAVIDWebService: a versatile R interface to DAVID. Bioinformatics *29*, 2810-2811.

Freund, A., Laberge, R.M., Demaria, M., and Campisi, J. (2012). Lamin B1 loss is a senescence-associated biomarker. Mol Biol Cell *23*, 2066-2075.

Gonen, N., Sabath, N., Burge, C.B., Shalgi, R. (2019). Widespread PERK-dependent repression of ER targets in response to ER stress. bioRxiv *487934*.

Guan, B.J., van Hoef, V., Jobava, R., Elroy-Stein, O., Valasek, L.S., Cargnello, M., Gao, X.H., Krokowski, D., Merrick, W.C., Kimball, S.R.*, et al.* (2017). A Unique ISR Program Determines Cellular Responses to Chronic Stress. Molecular cell *68*, 885-900 e886.

Haigis, M.C., and Yankner, B.A. (2010). The aging stress response. Molecular cell *40*, 333-344.

Hall, D.M., Xu, L., Drake, V.J., Oberley, L.W., Oberley, T.D., Moseley, P.L., and Kregel, K.C. (2000). Aging reduces adaptive capacity and stress protein expression in the liver after heat stress. J Appl Physiol (1985) *89*, 749-759.

Hartl, F.U., Bracher, A., and Hayer-Hartl, M. (2011). Molecular chaperones in protein folding and proteostasis. Nature *475*, 324-332.

Heydari, A.R., Wu, B., Takahashi, R., Strong, R., and Richardson, A. (1993). Expression of heat shock protein 70 is altered by age and diet at the level of transcription. Mol Cell Biol *13*, 2909-2918.

Ingolia, N.T., Brar, G.A., Rouskin, S., McGeachy, A.M., and Weissman, J.S. (2012). The ribosome profiling strategy for monitoring translation in vivo by deep sequencing of ribosome-protected mRNA fragments. Nature protocols *7*, 1534-1550.

Ivanov, A., Pawlikowski, J., Manoharan, I., van Tuyn, J., Nelson, D.M., Rai, T.S., Shah, P.P., Hewitt, G., Korolchuk, V.I., Passos, J.F.*, et al.* (2013). Lysosome-mediated processing of chromatin in senescence. J Cell Biol *202*, 129-143.

Jolly, C., Konecny, L., Grady, D.L., Kutskova, Y.A., Cotto, J.J., Morimoto, R.I., and Vourc'h, C. (2002). In vivo binding of active heat shock transcription factor 1 to human chromosome 9 heterochromatin during stress. J Cell Biol *156*, 775-781.

Jolly, C., Usson, Y., and Morimoto, R.I. (1999). Rapid and reversible relocalization of heat shock factor 1 within seconds to nuclear stress granules. Proc Natl Acad Sci U S A *96*, 6769-6774.

Katz, Y., Wang, E.T., Airoldi, E.M., and Burge, C.B. (2010). Analysis and design of RNA sequencing experiments for identifying isoform regulation. Nat Methods *7*, 1009-1015.

Kregel, K.C., and Moseley, P.L. (1996). Differential effects of exercise and heat stress on liver HSP70 accumulation with aging. J Appl Physiol (1985) *80*, 547-551.

Labbadia, J., and Morimoto, R.I. (2015a). The biology of proteostasis in aging and disease. Annu Rev Biochem *84*, 435-464.

Labbadia, J., and Morimoto, R.I. (2015b). Repression of the Heat Shock Response Is a Programmed Event at the Onset of Reproduction. Molecular cell *59*, 639-650.

Langmead, B., and Salzberg, S.L. (2012). Fast gapped-read alignment with Bowtie 2. Nature methods *9*, 357-359.

Li, B., and Dewey, C.N. (2011). RSEM: accurate transcript quantification from RNA-Seq data with or without a reference genome. BMC Bioinformatics *12*, 323.

Liu, A.Y., Lin, Z., Choi, H.S., Sorhage, F., and Li, B. (1989). Attenuated induction of heat shock gene expression in aging diploid fibroblasts. J Biol Chem *264*, 12037-12045.

Locke, M. (2000). Heat shock transcription factor activation and hsp72 accumulation in aged skeletal muscle. Cell Stress Chaperones *5*, 45-51.

Locke, M., and Tanguay, R.M. (1996). Diminished heat shock response in the aged myocardium. Cell Stress Chaperones *1*, 251-260.

Lopez-Otin, C., Blasco, M.A., Partridge, L., Serrano, M., and Kroemer, G. (2013). The hallmarks of aging. Cell *153*, 1194-1217.

Love, M.I., Huber, W., and Anders, S. (2014). Moderated estimation of fold change and dispersion for RNA-seq data with DESeq2. Genome Biol *15*, 550.

Merkwirth, C., Jovaisaite, V., Durieux, J., Matilainen, O., Jordan, S.D., Quiros, P.M., Steffen, K.K., Williams, E.G., Mouchiroud, L., Tronnes, S.U.*, et al.* (2016). Two Conserved Histone Demethylases Regulate Mitochondrial Stress-Induced Longevity. Cell *165*, 1209-1223.

Narita, M., Nunez, S., Heard, E., Narita, M., Lin, A.W., Hearn, S.A., Spector, D.L., Hannon, G.J., and Lowe, S.W. (2003). Rb-mediated heterochromatin formation and silencing of E2F target genes during cellular senescence. Cell *113*, 703-716.

O'Sullivan, R.J., Kubicek, S., Schreiber, S.L., and Karlseder, J. (2010). Reduced histone biosynthesis and chromatin changes arising from a damage signal at telomeres. Nat Struct Mol Biol *17*, 1218-1225.

Pavitt, G.D., and Ron, D. (2012). New insights into translational regulation in the endoplasmic reticulum unfolded protein response. Cold Spring Harb Perspect Biol *4*.

Prokocimer, M., Barkan, R., and Gruenbaum, Y. (2013). Hutchinson-Gilford progeria syndrome through the lens of transcription. Aging Cell *12*, 533-543.

Rai, T.S., Cole, J.J., Nelson, D.M., Dikovskaya, D., Faller, W.J., Vizioli, M.G., Hewitt, R.N., Anannya, O., McBryan, T., Manoharan, I.*, et al.* (2014). HIRA orchestrates a dynamic chromatin landscape in senescence and is required for suppression of neoplasia. Genes Dev *28*, 2712-2725.

Reid, D.W., Chen, Q., Tay, A.S., Shenolikar, S., and Nicchitta, C.V. (2014). The unfolded protein response triggers selective mRNA release from the endoplasmic reticulum. Cell *158*, 1362-1374.

Sen, P., Shah, P.P., Nativio, R., and Berger, S.L. (2016). Epigenetic Mechanisms of Longevity and Aging. Cell *166*, 822-839.

Shah, P.P., Donahue, G., Otte, G.L., Capell, B.C., Nelson, D.M., Cao, K., Aggarwala, V., Cruickshanks, H.A., Rai, T.S., McBryan, T.*, et al.* (2013). Lamin B1 depletion in senescent cells triggers large-scale changes in gene expression and the chromatin landscape. Genes Dev *27*, 1787-1799.

Shai, N., Shemesh, N., and Ben-Zvi, A. (2014). Remodeling of Proteostasis Upon Transition to Adulthood is Linked to Reproduction Onset. Curr Genomics *15*, 122-129.

Shalgi, R., Hurt, J.A., Krykbaeva, I., Taipale, M., Lindquist, S., and Burge, C.B. (2013). Widespread regulation of translation by elongation pausing in heat shock. Molecular cell *49*, 439-452.

Shalgi, R., Hurt, J.A., Lindquist, S., and Burge, C.B. (2014). Widespread Inhibition of Posttranscriptional Splicing Shapes the Cellular Transcriptome following Heat Shock. Cell reports *7*, 1362-1370.

Shemesh, N., Shai, N., and Ben-Zvi, A. (2013). Germline stem cell arrest inhibits the collapse of somatic proteostasis early in Caenorhabditis elegans adulthood. Aging Cell *12*, 814-822.

Shimi, T., Butin-Israeli, V., Adam, S.A., Hamanaka, R.B., Goldman, A.E., Lucas, C.A., Shumaker, D.K., Kosak, S.T., Chandel, N.S., and Goldman, R.D. (2011). The role of nuclear lamin B1 in cell proliferation and senescence. Genes Dev *25*, 2579-2593.

Shoulders, M.D., Ryno, L.M., Genereux, J.C., Moresco, J.J., Tu, P.G., Wu, C., Yates, J.R., 3rd, Su, A.I., Kelly, J.W., and Wiseman, R.L. (2013). Stress-independent activation of XBP1s and/or ATF6 reveals three functionally diverse ER proteostasis environments. Cell Rep *3*, 1279-1292.

Taylor, R.C., and Dillin, A. (2011). Aging as an event of proteostasis collapse. Cold Spring Harb Perspect Biol *3*.

Taylor, R.C., and Dillin, A. (2013). XBP-1 is a cell-nonautonomous regulator of stress resistance and longevity. Cell *153*, 1435-1447.

Vilchez, D., Saez, I., and Dillin, A. (2014). The role of protein clearance mechanisms in organismal ageing and age-related diseases. Nat Commun *5*, 5659.

Westerheide, S.D., Anckar, J., Stevens, S.M., Jr., Sistonen, L., and Morimoto, R.I. (2009). Stress-inducible regulation of heat shock factor 1 by the deacetylase SIRT1. Science *323*, 1063-1066.

Wood, J.G., Hillenmeyer, S., Lawrence, C., Chang, C., Hosier, S., Lightfoot, W., Mukherjee, E., Jiang, N., Schorl, C., Brodsky, A.S.*, et al.* (2010). Chromatin remodeling in the aging genome of Drosophila. Aging Cell *9*, 971-978.

Zelin, E., and Freeman, B.C. (2015). Lysine deacetylases regulate the heat shock response including the age-associated impairment of HSF1. J Mol Biol *427*, 1644-1654.

Zhang, K., and Kaufman, R.J. (2004). Signaling the unfolded protein response from the endoplasmic reticulum. J Biol Chem *279*, 25935-25938.

Figure 1

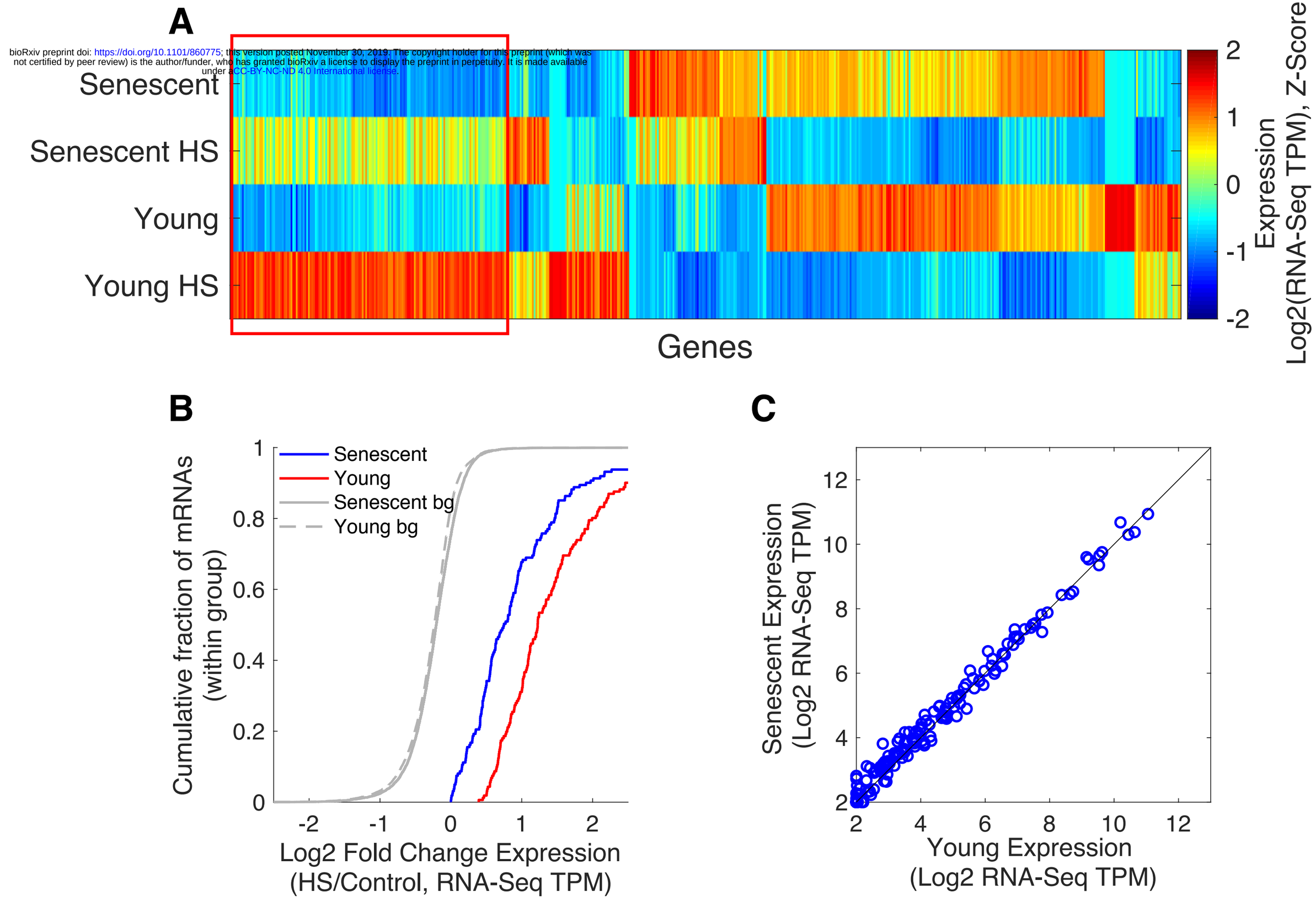

Figure 2

A

Category	Term	Count	FDR
GOTERM_BP_DIRECT	GO:0006986~response to unfolded protein	17	5.64E-16
UP_KEYWORDS	Stress response	20	3.18E-15
GOTERM_MF_DIRECT	GO:0051082~unfolded protein binding	17	8.85E-10
UP_KEYWORDS	Chaperone	21	1.57E-09
INTERPRO	IPR013126:Heat shock protein 70 family	9	8.97E-09
INTERPRO	IPR018181:Heat shock protein 70, conserved site	9	8.97E-09
GOTERM_BP_DIRECT	GO:0042026~protein refolding	9	1.56E-08
KEGG_PATHWAY	hsa04141:Protein processing in endoplasmic reticulum	20	2.14E-08
GOTERM_MF_DIRECT	GO:0051087~chaperone binding	13	9.55E-07
GOTERM_BP_DIRECT	GO:1900034~regulation of cellular response to heat	13	1.92E-06
GOTERM_BP_DIRECT	GO:0006457~protein folding	16	1.30E-05
GOTERM_BP_DIRECT	GO:0031396~regulation of protein ubiquitination	7	6.53E-05
GOTERM_MF_DIRECT	GO:0031072~heat shock protein binding	9	1.38E-04
KEGG_PATHWAY	hsa04612:Antigen processing and presentation	8	0.005318005
GOTERM_BP_DIRECT	GO:0009408~response to heat	7	0.010453571

B

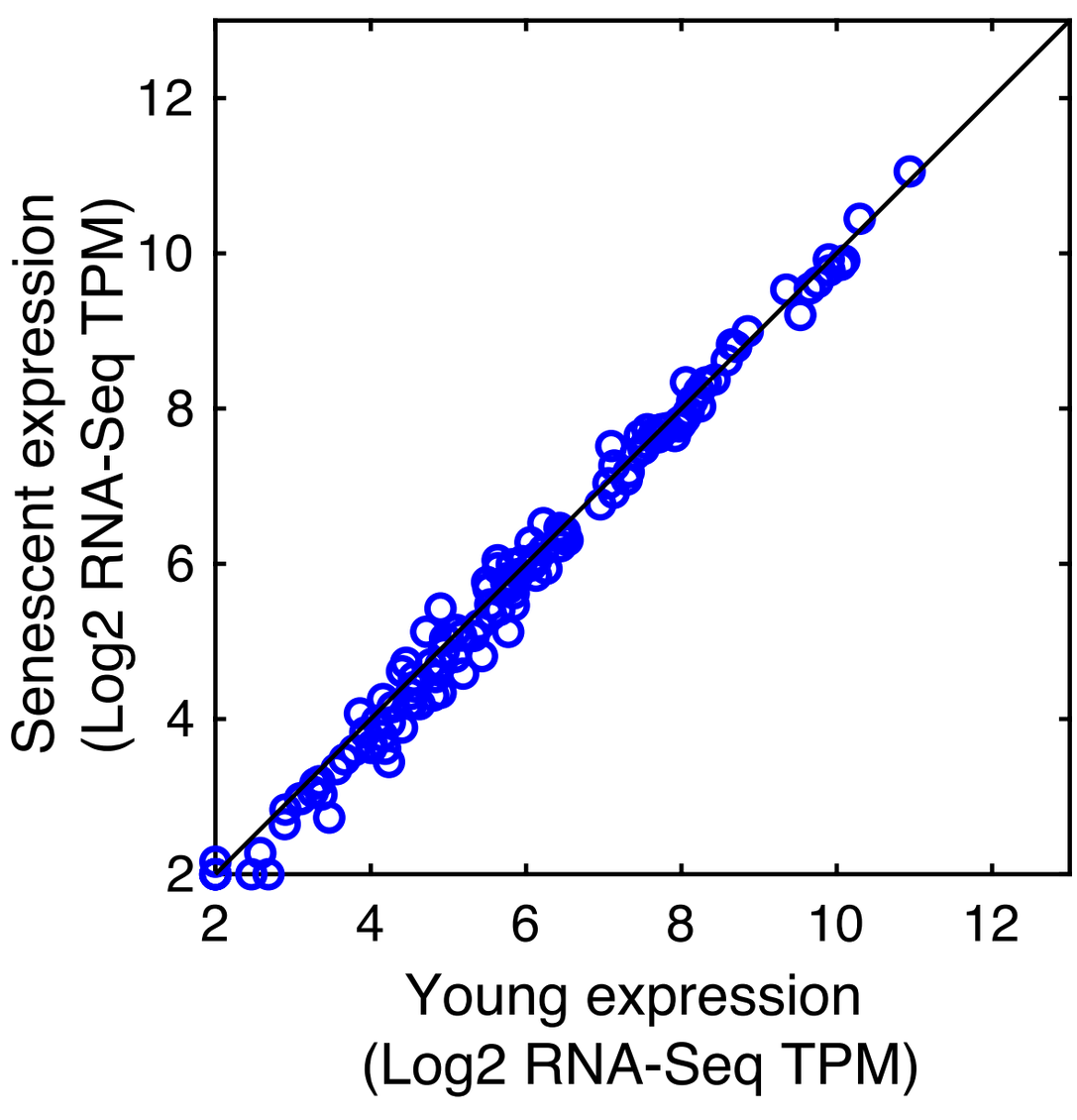

C

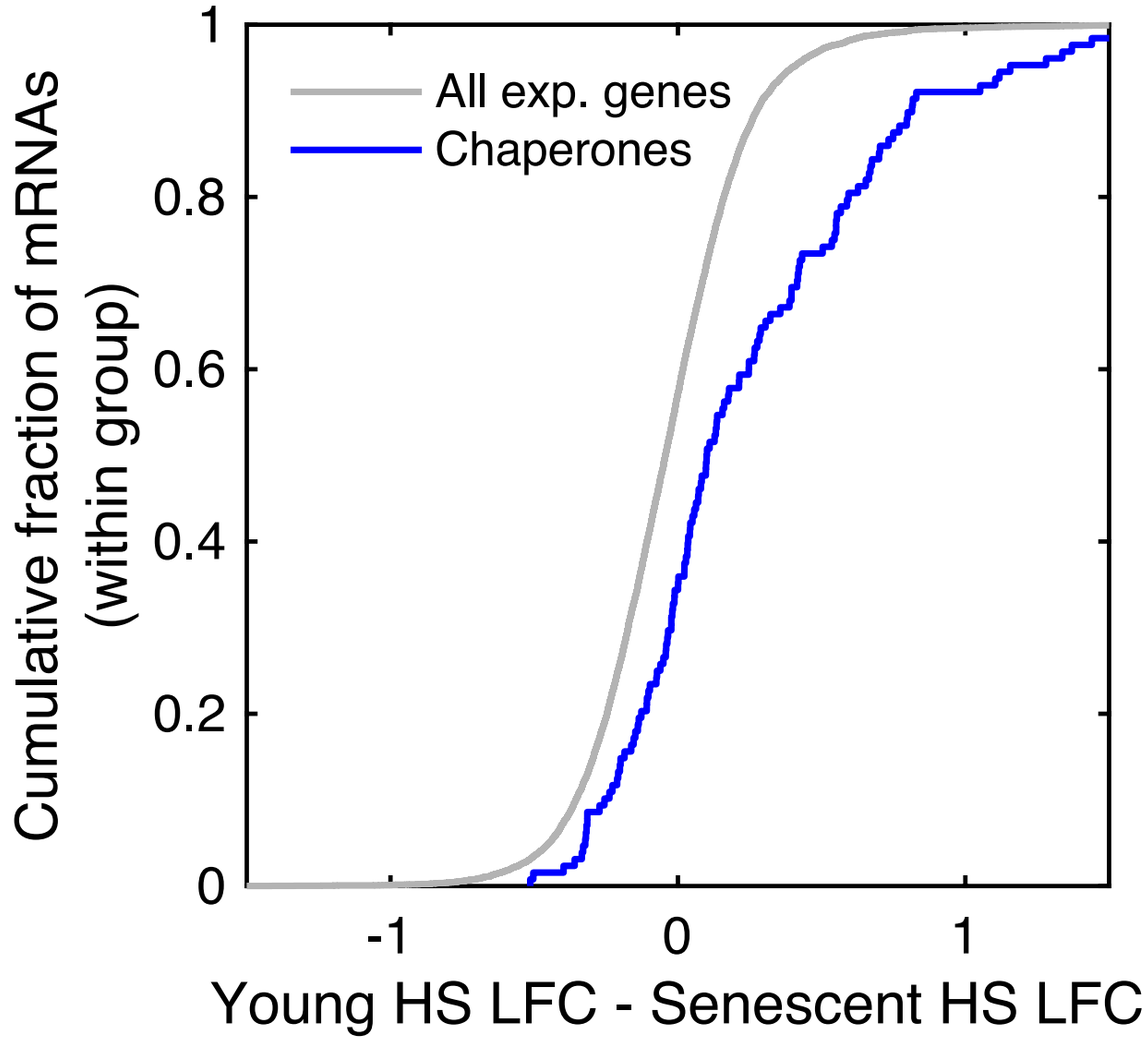

Figure 3

A.

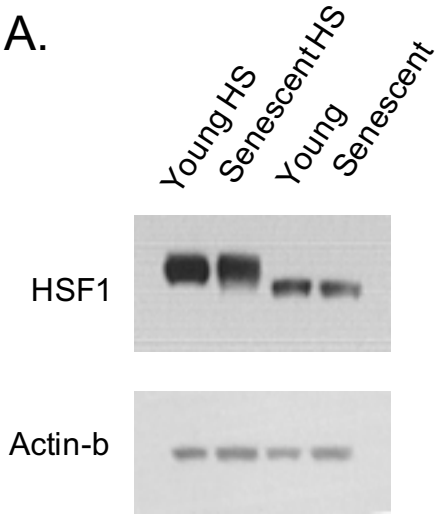
Young HS
Senescent HS
Young
Senescent
HSF1
Actin-b

B.

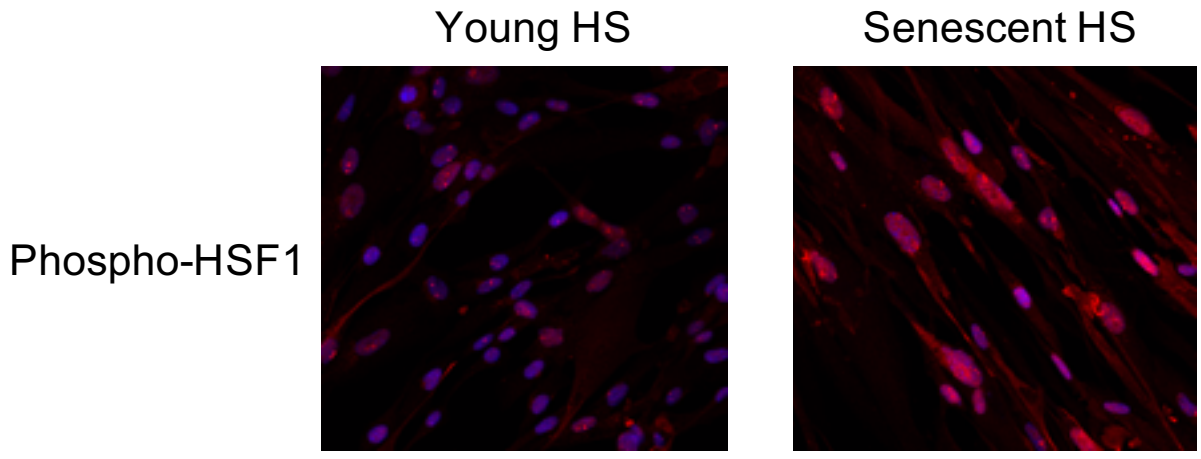
Young HS
Senescent HS
Phospho-HSF1

C.

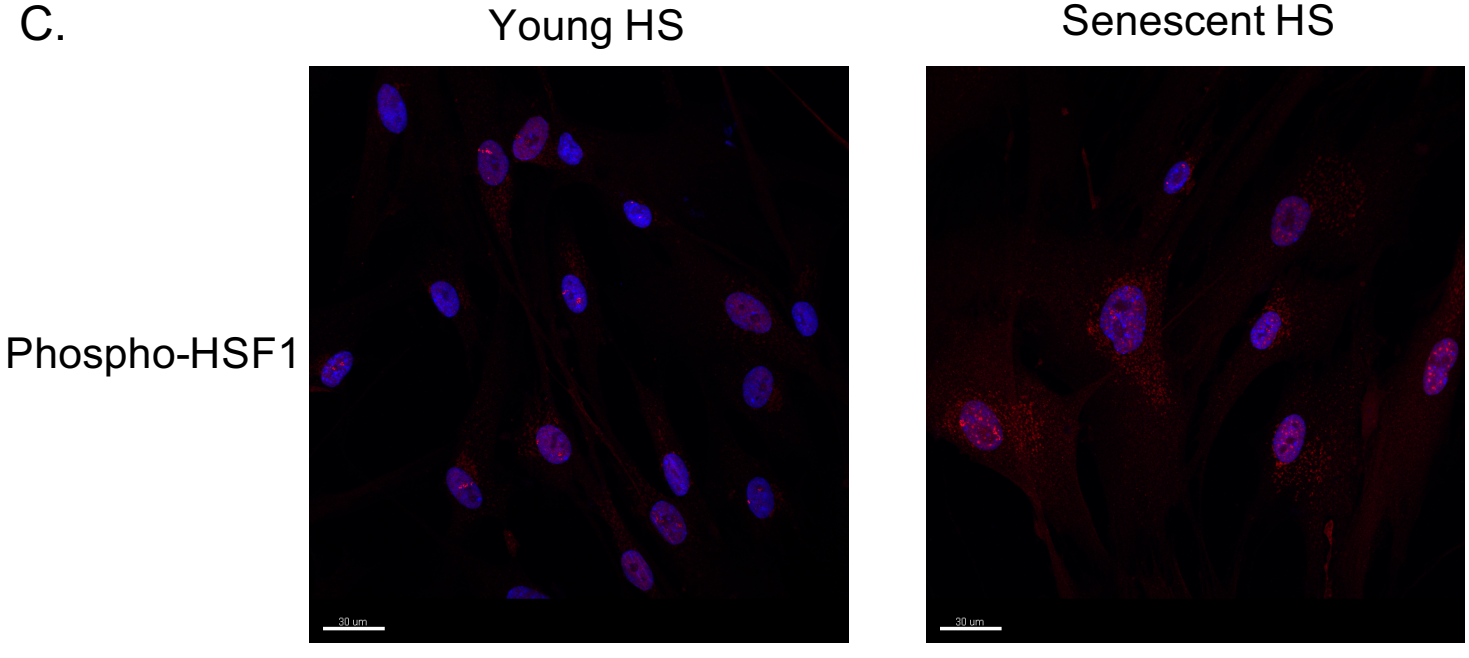
Young HS
Senescent HS
Phospho-HSF1
30 um
30 um

Figure 4

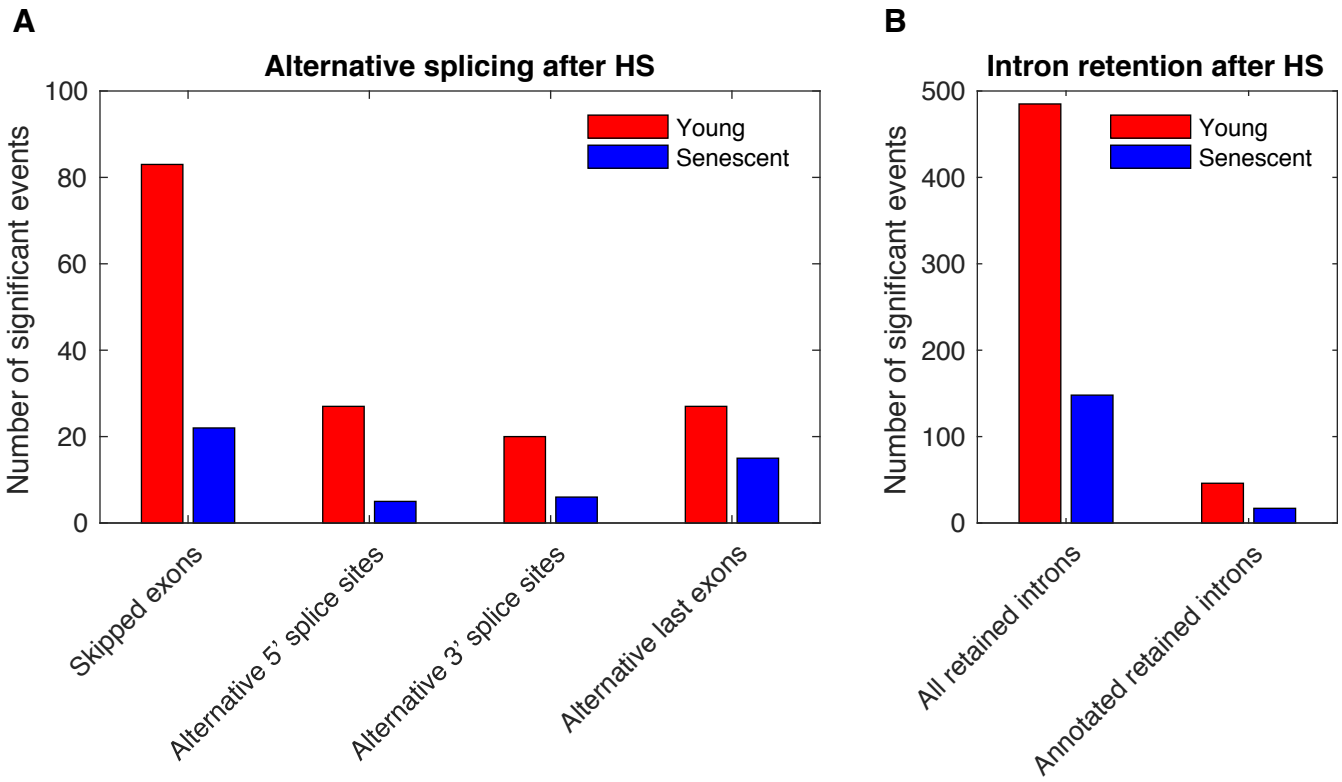

Figure 5

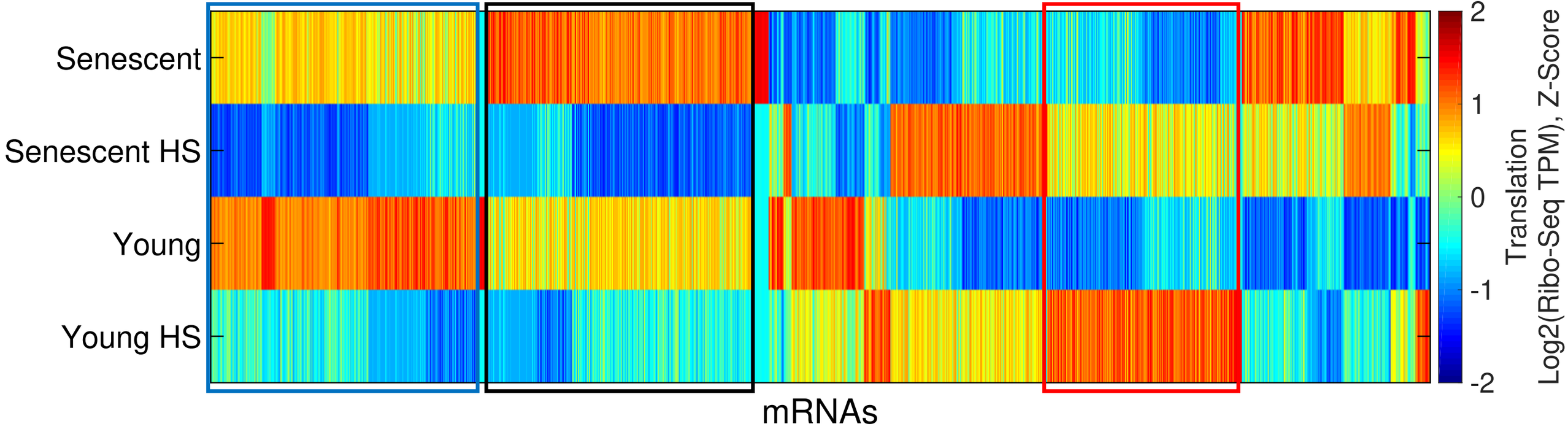
Senescent
Senescent HS
Young
Young HS
mRNAs
2
1
0
-1
-2
Translation
Log2(Ribo-Seq TPM), Z-Score

Figure 6

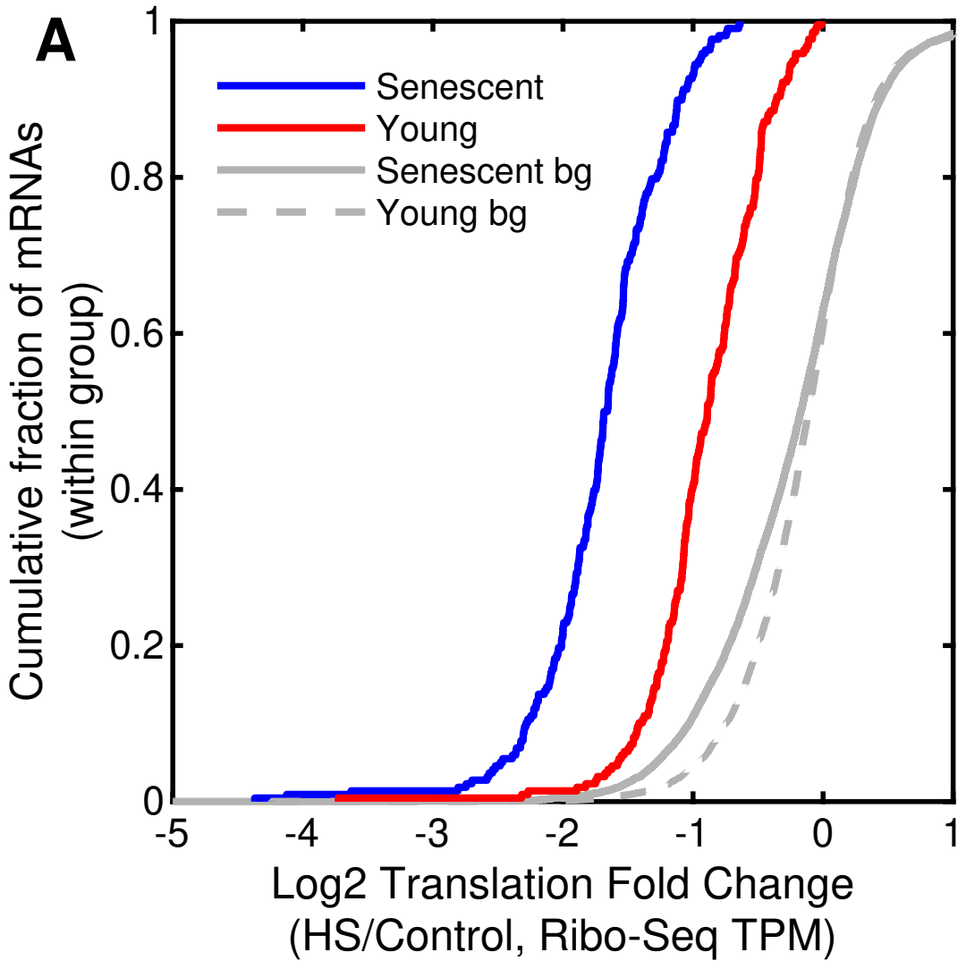

B

Category	Term	Count	FDR
UP_SEQ_FEATURE	glycosylation site:N-linked (GlcNAc...)	76	6.38E-09
UP_SEQ_FEATURE	signal peptide	66	4.33E-08
UP_KEYWORDS	Membrane	142	8.48E-08
UP_KEYWORDS	Disulfide bond	59	1.09E-07
UP_KEYWORDS	Signal	76	1.40E-07
UP_KEYWORDS	Glycoprotein	77	3.94E-07
UP_SEQ_FEATURE	topological domain:Extracellular	47	2.12E-06
UP_SEQ_FEATURE	transmembrane region	91	2.18E-05
UP_KEYWORDS	Transmembrane	100	2.87E-05
UP_KEYWORDS	Cell membrane	56	1.27E-04
GOTERM_CC_DIRECT	GO:0005886~plasma membrane	75	3.21E-04
UP_KEYWORDS	Receptor	29	4.63E-04
GOTERM_CC_DIRECT	GO:0005887~integral component of plasma membrane	30	0.007968
GOTERM_BP_DIRECT	GO:0007229~integrin-mediated signaling pathway	10	0.016856
UP_SEQ_FEATURE	disulfide bond	40	0.018386
GOTERM_CC_DIRECT	GO:0016021~integral component of membrane	87	0.018925
GOTERM_BP_DIRECT	GO:0043547~positive regulation of GTPase activity	23	0.02586
GOTERM_BP_DIRECT	GO:0007165~signal transduction	34	0.037182

C

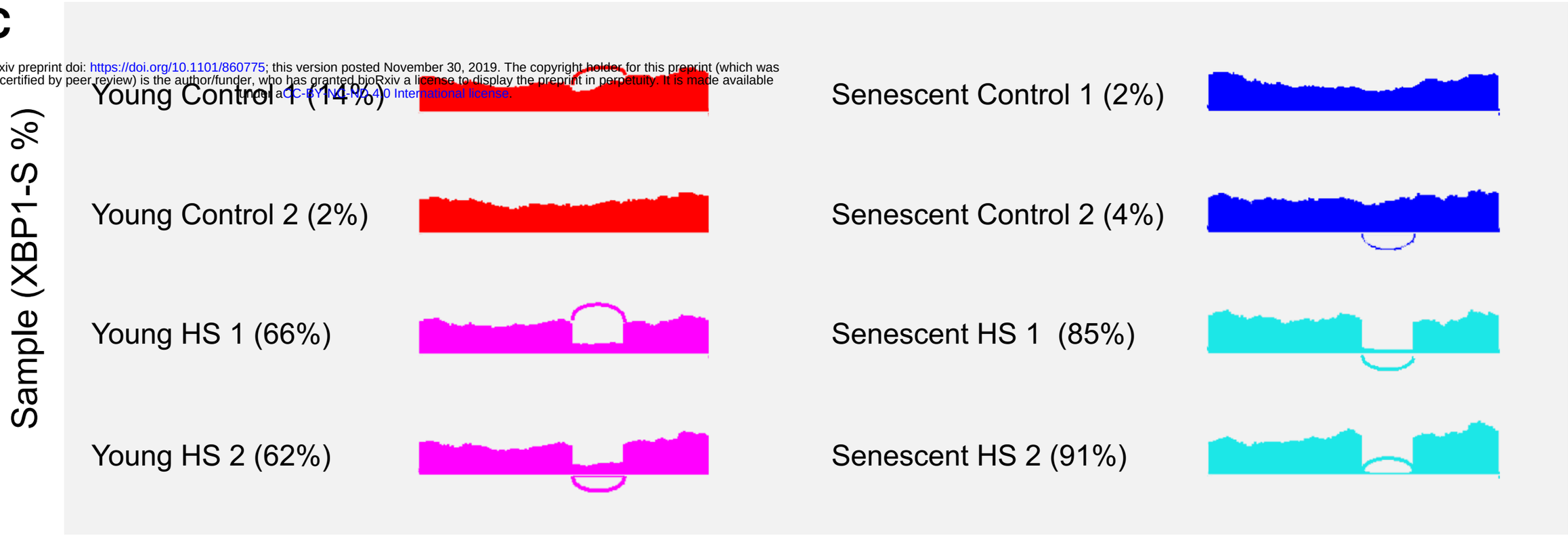

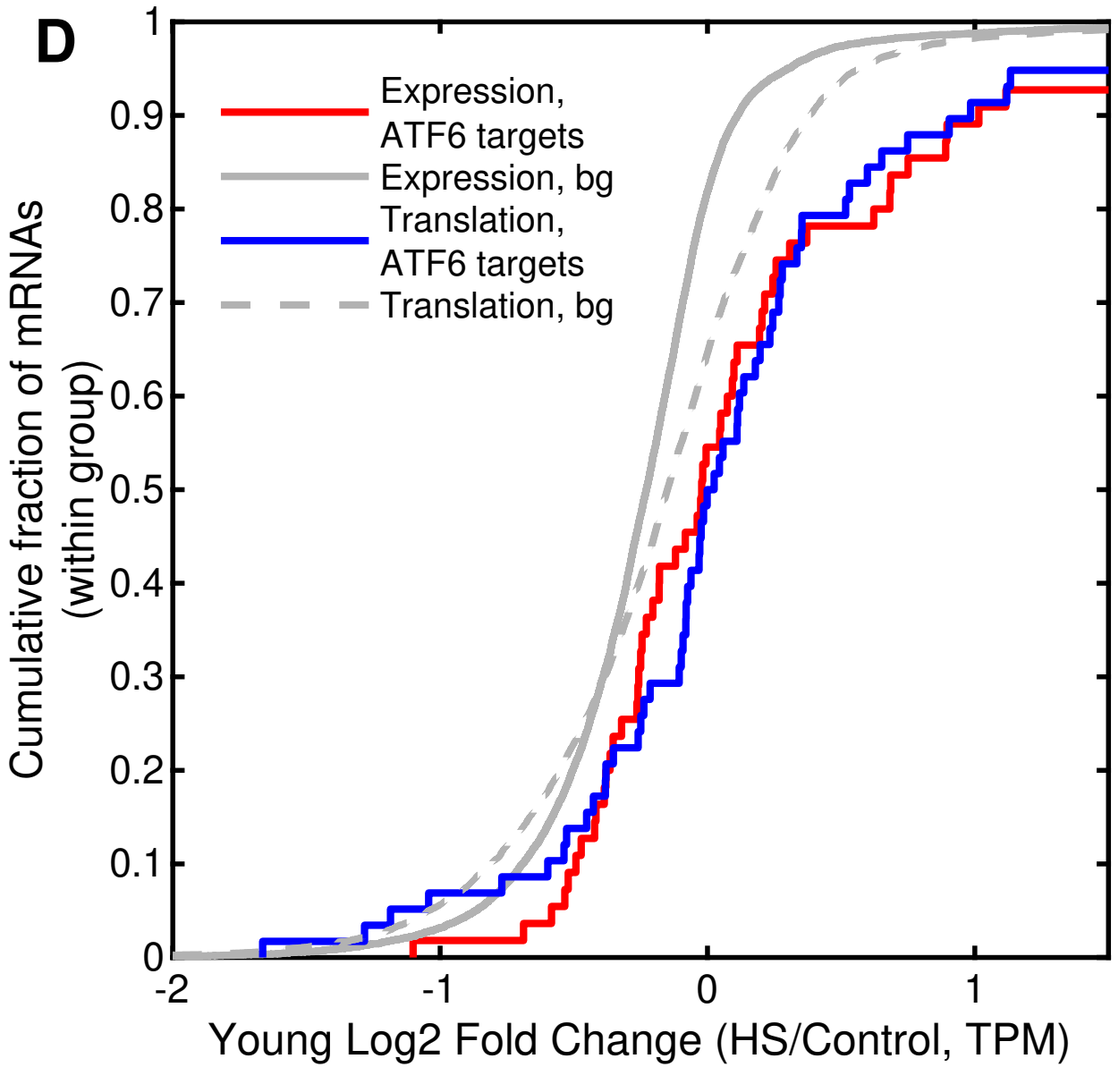

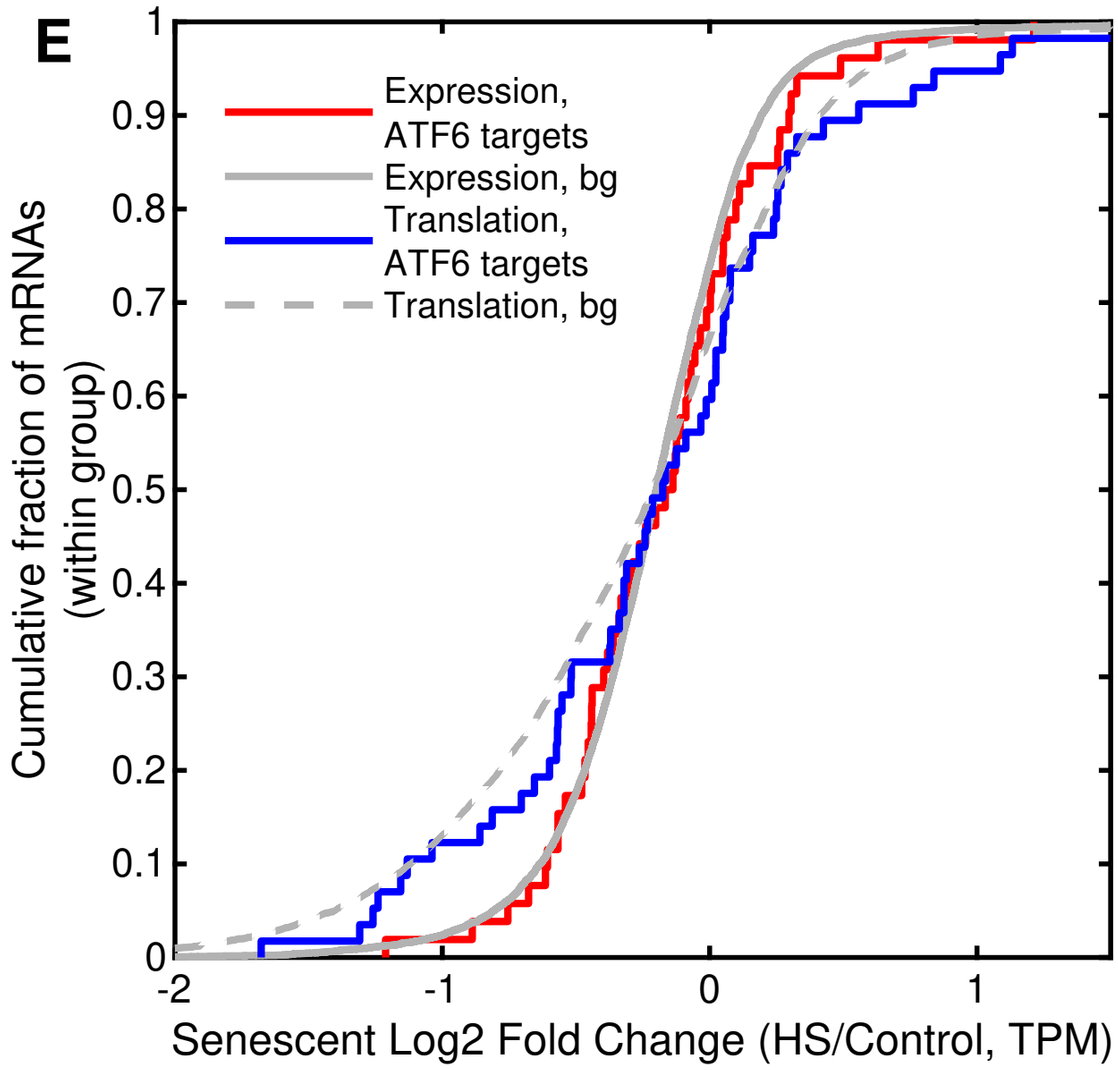

Figure 7

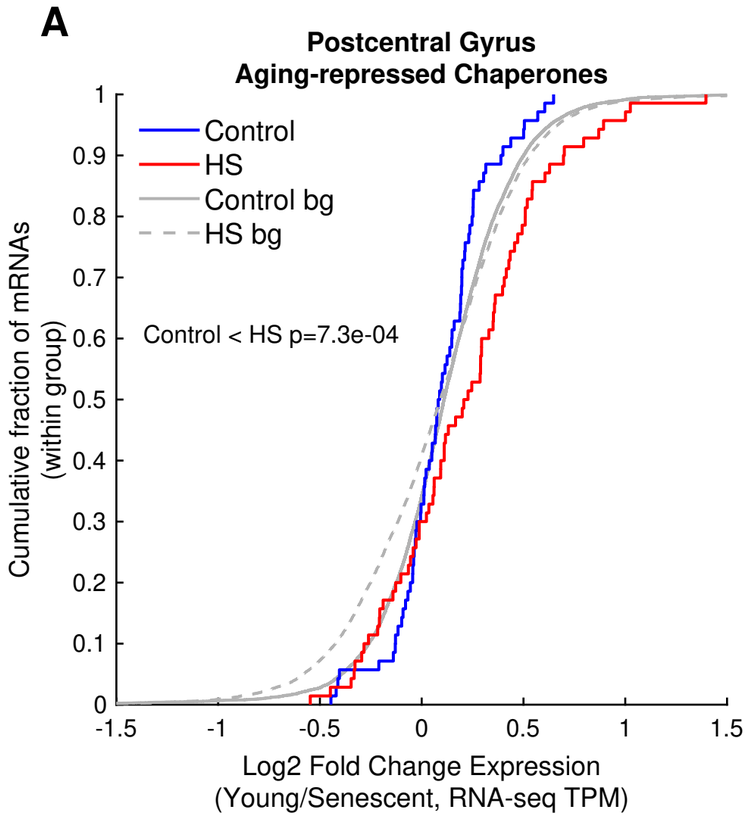
A
Postcentral Gyrus
Aging-repressed Chaperones
Control
HS
Control bg
HS bg
Control < HS p=7.3e-04
Cumulative fraction of mRNAs (within group)
Log2 Fold Change Expression (Young/Senescent, RNA-seq TPM)

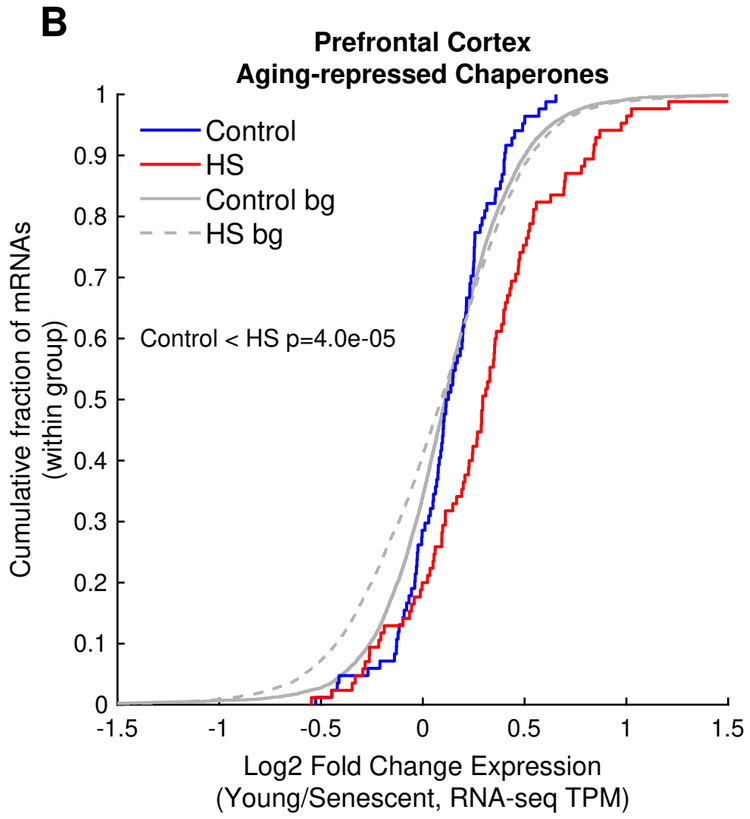
B
Prefrontal Cortex
Aging-repressed Chaperones
Control
HS
Control bg
HS bg
Control < HS p=4.0e-05
Cumulative fraction of mRNAs (within group)
Log2 Fold Change Expression (Young/Senescent, RNA-seq TPM)

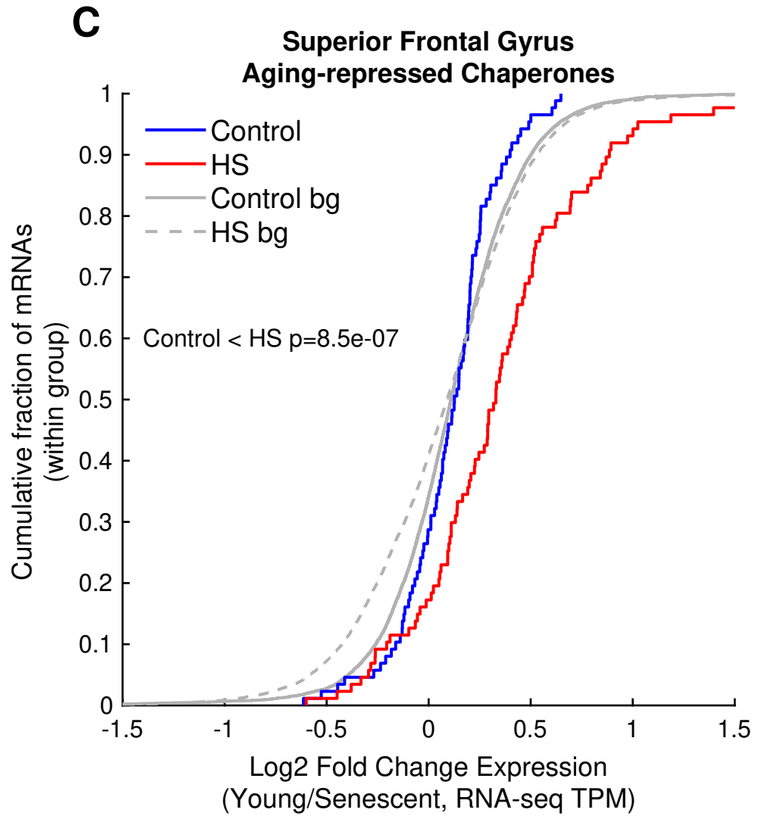
C
Superior Frontal Gyrus
Aging-repressed Chaperones
Control
HS
Control bg
HS bg
Control < HS p=8.5e-07
Cumulative fraction of mRNAs (within group)
Log2 Fold Change Expression (Young/Senescent, RNA-seq TPM)